Received: 27 August 2021 | Revised: 28 December 2021 | Accepted: 30 December 2021

DOI: 10.1111/joa.13623

Journal of Anatomy ANATOMICAL SOCIETY WILEY

ORIGINAL PAPER

Morphology of joints and patterns of cartilage calcification in the endoskeleton of the batoid *Raja* cf. *polystigma*

Ugo E. Pazzaglia[1] | Marcella Reguzzoni[2] | Renata Manconi[3] | Piero Antonio Zecca[2] | Guido Zarattini[1] | Monica Campagnolo[4] | Mario Raspanti[2]

[1]DSMC, University of Brescia, Brescia, Italy

[2]DVM (Zoology Lab), University of Sassari, Sassari, Italy

[3]DMC, University of Insubria, Varese, Italy

[4]DBSV, University of Insubria, Varese, Italy

Correspondence
Ugo E. Pazzaglia, DSMC, University of Brescia, Brescia, Italy.
Email: u.e.pazzaglia@gmail.com

Abstract

The skeleton of the batoid fish consists of a mixture of calcified and uncalcified cartilage with a typical layout of mineral deposition toward the outer border, leaving an uncalcified central core in most of the skeleton segments. An exception is observed in the radials, where mineral deposition is central. Joints and endoskeleton segments were studied in two adult samples of *Raja* cf. *polystigma*. Histomorphology, mineral deposition pattern, and zonal chondrocyte duplication activity were compared among several endoskeleton segments, but with particular attention to the fin rays; in the first, the uncalcified cartilage is central with an outer layer ranging from mineralized tesserae to a continuous calcified coating, whereas in the second, the uncalcified cartilage surrounds one or more central calcified columns. The diarthroses have a joint cavity closed by a fibrous capsule and the sliding surfaces rest on the base of mineralized tesserae, whereas the interradial amphiarthroses show a layer of densely packed chondrocytes between the flat, calcified discs forming the base of neighboring radials. In the endoskeleton segments, three types of tesserae are distinguished, characterizing the phases of skeletal growth and mineralization which present differences in each endoskeleton segment. The chondrocyte density between central core, subtesseral layer, and radial external cartilage did not show significant differences, while there was a significant difference in chondrocyte density between the latter zones and the type c tesserae of the pelvic girdle. The histomorphology and morphometry observed in *Raja* cf. *polystigma* suggest a model of cartilage growth associated with structural stiffening without remodeling. A key point of this model is suggested to be the incomplete mineralization of the tesseral layer and the continuous growth of cartilage, both enabling fluid diffusion through the matrix fibril network of scattered, uncalcified cartilage zones inside and between the tesserae.

KEYWORDS
batoids, chondrocytes duplication, endoskeleton segments, mineralization pattern, radials, tesserae

 © 2022 Anatomical Society

1 | INTRODUCTION

The elasmobranch fishes are distinguished among extant vertebrates by the cartilaginous skeleton with a peculiar deposition pattern of the mineral deposition in the cartilage matrix, the "tesserae" (Clement, 1992; Dean & Summers, 2006; Hall, 2005; Kemp & Westrin, 1979). A specific trait of the *Chondrichthyes* skeletal segments is that they remain cartilaginous throughout life and are not replaced by bone tissue in fully grown fish. In mammalian skeletal anlagen, the cartilage matrix between hypertrophic chondrocyte undergoes calcification which serves as a scaffold for osteoblast deposition of osteoid (endochondral ossification). This mineralized tissue (a mixture of cartilage and primary bone) is then remodeled by replacing the calcified cartilage with bone matrix; thus, at end of the growth period, a cartilage layer can be observed only on the joint surface (Decker, 2017).

In mammalian ontogeny, chondrocyte proliferation is controlled by genes encoding the extracellular matrix (ECM), and upstream transcriptional regulators guide the growth and shaping of the embryonic cartilage model unlike chondrichthyans fishes (Marconi et al., 2020). In the fetal and postnatal periods, mineralization of cartilage also plays a complementary role in orienting the growth process (Pazzaglia et al., 2017). Calcification of the perichondral and intercolumnar matrix between chondrocytes is known to always be associated with an increase in chondrocyte volume, cytoplasmic vacuolization (hypertrophic chondrocytes), followed by apoptosis or necrosis of the cell, as can be observed in the epiphyseal ossification centers and in the metaphyseal growth plate of mammals, where the line of mineral deposition is always observed below the level at which chondrocytes hypertrophy starts (Pazzaglia et al., 2020). However, this is not the unique calcification pattern present in developing mammalian bone models because in the joint cartilage matrix, a thin base layer of mineral deposition is formed without evidence of chondrocyte hypertrophy.

In contrast to mammals, the cartilaginous fish calcification pattern enables continuous growth for the whole lifespan and, at the same time, provides mechanical stiffening of the skeletal segments. In batoids, a variable range of flexibility is adapted to the motion of these animals in the water column or on the seabed (Lucifora & Vassallo, 2002), suggesting that a morphofunctional role may be played by the endoskeleton calcification pattern. Moreover, it is remarkable in the latter the resemblance of the mobile joints with the diarthroses of mammalians in a structural calcified cartilage complex completely diverging from that of the endosteal bones. Indeed, the persistent hyaline cartilage skeleton of *Chondrichthyes* is stiffened by the superficial layer of calcified cartilage in the form of small, mineralized plates (tesserae), while the inner core remains cartilaginous without any evidence of endochondral ossification (Dean & Summers, 2006). This particular structural layout of mineral deposits satisfies the mechanical requirements of propterygia flexural stiffness for punting (Macesic & Summers, 2012) while providing graded flexibility to the "radial" segments adapted to the fish swimming modes (Schaefer & Summers, 2005).

The tesseral morphology and this pattern of mineral deposition in elasmobranch cartilage have been investigated extensively with the application of high-resolution 2D and 3D microcomputed tomography and structural characterization of the calcified material. They have suggested a series of distinct phases of mineralization of the tesserae that form the first isolated, globular islets of mineralized cartilage that increase in size with the age of the fish and come into contact with each other to form a more complete tesseral surface of the mature cartilaginous skeleton (Seidel et al., 2016; Seidel, Blumer, Pechriggi, 2017; Seidel, Blumer, Zoslansky, 2017). Despite the large variation in the shape and size of the tesserae, these are observed among species of all the major elasmobranch groups (Dean & Summers, 2006; Maisey et al., 2020; Seidel, Blumer, et al., 2020; Seidel, Jayasankar, et al., 2020) to play in the endoskeleton of these fish the analogous, mechanical function of the bones in the tetrapods. However, no specific attention has been paid to comparing the mineral deposition in cartilaginous fish with that of mammalian endochondral ossification, where calcification has been extensively documented to be associated with chondrocytes transformation, such as hypertrophy (Pazzaglia et al., 2018, 2020). This has left the question of the mechanism of calcium and phosphorus concentration and Ca_2PO_4 nucleation in the cartilage ECM of elasmobranchs endoskeleton segments unanswered.

In this study conducted on the adult batoid *Raja* cf. *polystigma*, the skeletal morphology and histology of the calcification process in this species have been investigated with a comparative approach toward the endochondral ossification model. Our goals were to document: (1) the joint morphology and range of functional performance, (2) the variable pattern and topographic distribution of mineral deposition in the skeletal segments, (3) the variance of the tesserae morphology, and (4) the cartilage vascular supply and ECM ultrastructure for interstitial fluid diffusion and zonal distribution of chondrocyte duplication.

2 | MATERIALS AND METHODS

The study was carried out on two male specimens of *Raja* cf. *polystigma*, Regan, 1923; Chondrichthyes: Elasmobranchii: Batoidea: Rajiformes: Rajidae (Serena et al., 2010), captured in the Sardinia sea, western Mediterranean. This study complied with all ethical requirements of the *Journal of Anatomy* and local authorities. The specimens (weight 0.730 and 0.820 kg, respectively) were purchased from commercial sources (Fish Market), and animal welfare laws, guidelines, and policies were not applicable. The tissue specimens for the study were dissected within 24 h after capture, dividing the right- and left-wing fins (with the respective basals and radials) from the body and tail, immediately fixed in 10% buffered formaldehyde solution for 2 weeks, and then conserved until processing in a 4% solution of the same fixative at 5°C.

2.1 | Preparation and selection of anatomical specimens

X-rays of the wings, body, and tail were taken in the dorsoventral projection, whereas computerized tomography (CT) of the right

pelvic basipterygium was performed separately using a New Tom Cone Bean CT technology (New Tom). The upper and lower jaws and, pectoral and pelvic girdle were dissected under a low-power stereomicroscope (Olympus SZX7, Olympus Ltd). The joints between the pectoral girdle and propterygium and metapterygium, the pelvic girdle and basipterygium, and the compound radial were opened to expose the joint surface and a segment of the corresponding endoskeleton segments. The pterygia were dissected from the muscles for their entire length and smaller specimens (2 x 3 cm) of the fin zones (including median, intermediate, and distal radials) were divided with a scalpel and high-definition X-rays were obtained in the anteroposterior projection.

2.2 | Histomorphology and morphometry

Specimens of the upper and lower jaw, pectoral and pelvic girdle, pterygia, and radials were decalcified in a solution of acetic-hydrochloric acid (2% CH_3HCOOH/2% HCl) for 2 weeks, dehydrated in increasingly concentrated ethanol–water solutions, and embedded in paraffin. Transverse and longitudinal sections 7 μm in thickness were cut with a sledge microtome and stained with hematoxylin–eosin, May-Grunwald-Giemsa, PAS, and Alcian blue. Other fixed, undecalcified specimens were embedded in Technovit 7200 resin (Kulzer GmbH) and 150–200-μm-thick sections were prepared using the Exakt cutting/grinding system (Exakt Advanced Technology GmbH) and stained with von Kossa or methylene blue-acid fuchsine. The slides were observed using an Olympus BX 51 microscope (Olympus Ltd).

Morphometry was carried out on both undecalcified, thick sections (resin-embedded) stained with von Kossa, methylene blue-acid fuchsine and decalcified, thin sections (paraffin-embedded) stained with hematoxylin–eosin: (1) for the first group, three consecutive undecalcified cross-sections of the left basipterygium (Figure 1 segment 5, including the ventral and the two symmetric dorsal marginals) were selected to compare the mean height of the tesserae and the calcified flat peripheral layer of the dorsal marginals (Figure 2a) and the height of each tessera was measured, while in the segments with an unbroken calcified periphery, the thickness of the calcified layer was measured at regular intervals of 1 mm. (2) For the second group, decalcified transverse sections of the propterygium cartilage core were analyzed to assess the zonal chondrocyte density in this endoskeleton segment. The cell duplication rate in tissues could be assessed using a rapid technique for differential staining of mitotic cells in tumors, as documented with a combination of the acid Giemsa technique and counterstaining (Dooley et al., 1989). However, even in fetal mammalian cartilage models, rare cell mitosis requiring intensive effort at fairly high magnification to ensure correct identification is not applicable in these *Raja* cf. *polystigma* slides; therefore, we chose to assess in each area of interest the lacuna density, including those with two chondrocytes + the paired chondrocyte lacunae (defined by distance ≤10 μm between the lacunae) whose density was assumed as the index of recently occurring mitoses (Pazzaglia et al., 2017). A series

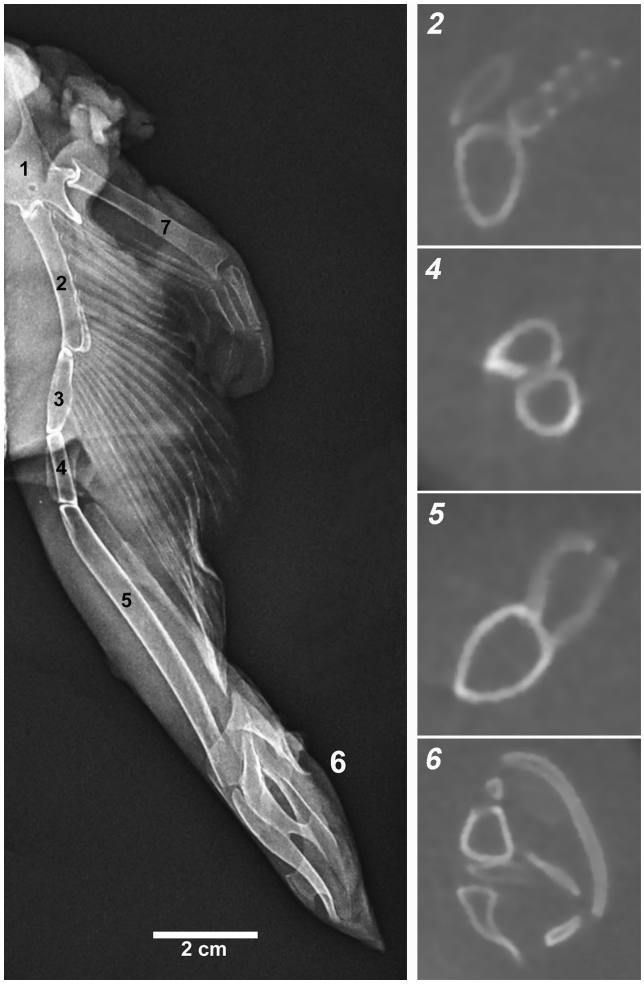

FIGURE 1 *Raja* cf. *polystigma* X-rays of the entire basipterygium and CT transverse sections of the corresponding segments: 1 pelvic girdle, 2–3 segments articulating with the pelvic radials, 4 intermediate segments, 5 axial, ventral, and dorsal marginals, and 6 clasper, compound radial (Compagno, 1999)

of randomized rectangular fields was acquired at a magnification of 200x (field area = 0.14 mm^2) with a Color View IIIb digital camera (Soft Imaging System GmbH). The number of chondrocyte lacunae with two cells inside + paired lacunae was counted using the program Cell (Soft Imaging System GmbH). The zonal chondrocyte density was compared between the metapterygium central core (a) and the other following zones: (b) the subtesseral, uncalcified cartilage layer (height approximately 500 μm below the tesserae) and (c) the uncalcified outer layer of the radials. A further comparison of the chondrocyte density was carried out on calcified cartilage of type **c** tesserae in the pelvic girdle (Figure 2d). Repeated counting of chondrocyte density was obtained independently by two investigators (MR and GZ) from a sample of 30% of the total histologic field equally distributed among the four zones. The difference in the mean analysis (Bland & Altman, 2010) was applied to these data sets. The difference between each paired measurement (intraobserver and interobserver) was plotted against the differences of the observers. By analyzing the difference between the paired

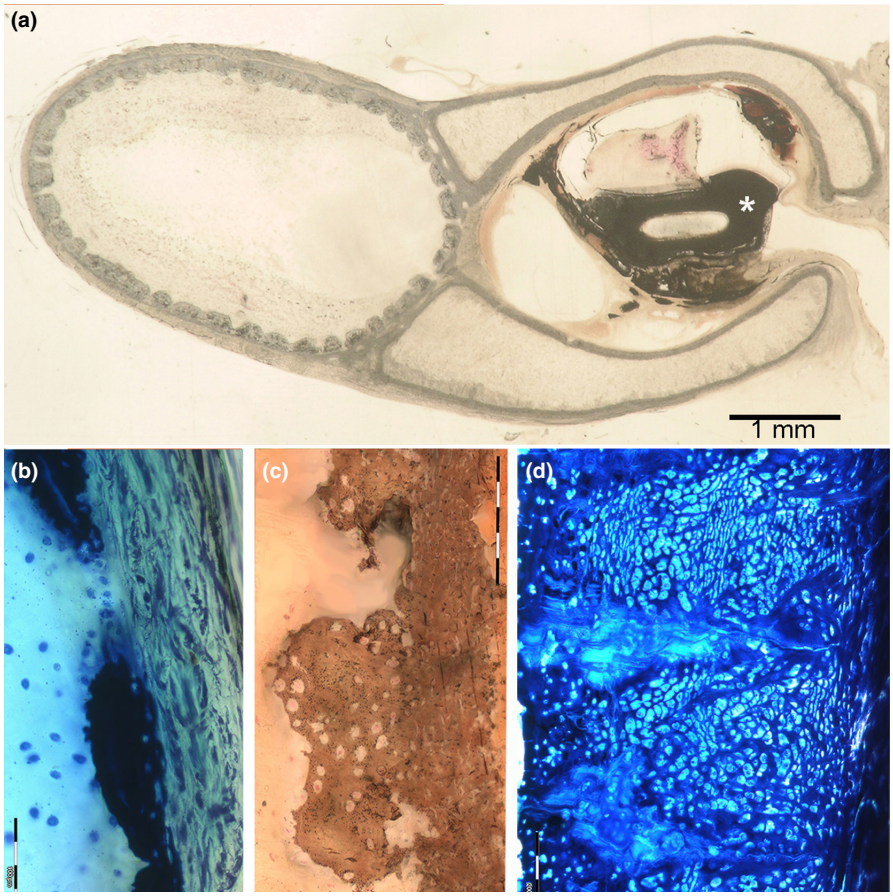

FIGURE 2 Histo-morphology of tessellated and not-tessellated endoskeleton segments in *Raja* cf. *polystigma*. (a) Resin-embedded, thick section of basipterygium segment 5, von Kossa, 1.5x. The axial segment shows a complete tessellated pattern and is distinct from the ventral and dorsal marginals with the not-tessellated, external layer. The latter delimit an open central space inside the ductus deferens (asterisk). (b) Resin-embedded, transverse thick section of metapterygium, methylene blue-acid fuchsine, 200x. Type a tessera in the early developmental stage inside of the perichondrial layer. (c) Resin-embedded, transverse thick section of propterygium, von Kossa, 200x. Type b tessera showing a basal layer of a denser calcified matrix, where can be recognized with difficulty flattened chondrocyte lacunae and a cup abutting toward the central core with larger globular lacunae with inside chondrocytes, suggesting a phasic tesseral size growth. (d) Resin-embedded, transverse thick section of the pelvic girdle, methylene blue-acid fuchsine, 200x. Type **c** tesserae are characterized by a very larger size than types a and b as well as by a higher chondrocytes density, alternating layers of globular (larger) and flattened lacunae (smaller)

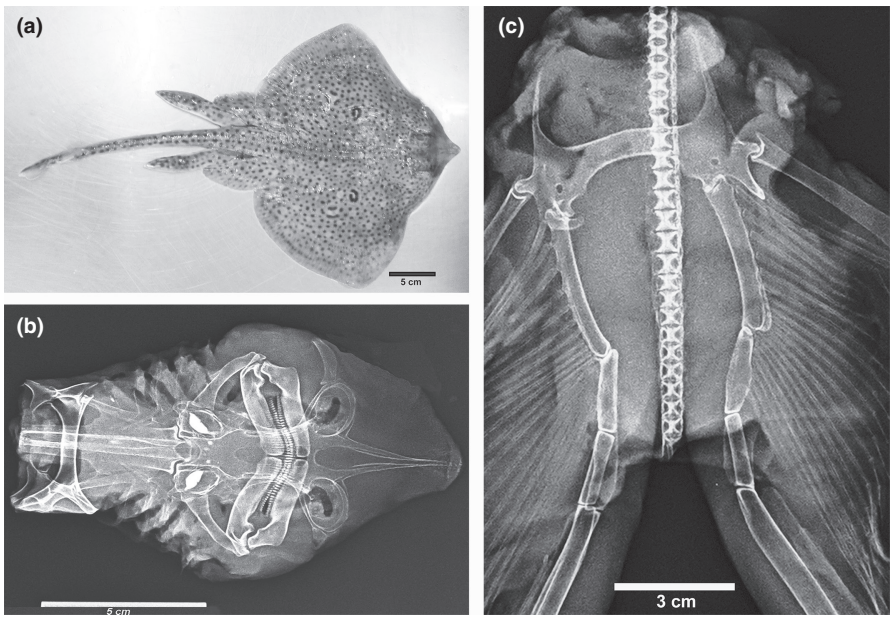

FIGURE 3 (a) Image of the male sample of *Raja* cf. *polystigma* (dorsal view). (b) X-ray of the dissected anterior endoskeleton showing the upper and lower jaw, hyomandibula, cervicothoracic synarcua, and thoracic girdle with the related joints. c) X-ray of the pelvic girdle, basipterygia, and spine. The ball-socked joint between pelvic girdle-compound radial and the condylar joint between pelvic girdle-basipterygium first segment and the other intersegmental joints are well evident as well as those between the pelvic radials and the first two basipterygium segments

measurements, the only source of variability was the measurement error, which was likely to follow a normal distribution. The variation in the differences for all the parameters tested was wider in the interobserver paired data sets than in the corresponding intraobserver set; however, with a degree of agreement >95% in confidence interval for both. Statistical analysis was performed using the MedCalc program (MedCalc Software) with the Student's *t* test for unpaired data. Statistical significance was set at $p < 0.05$.

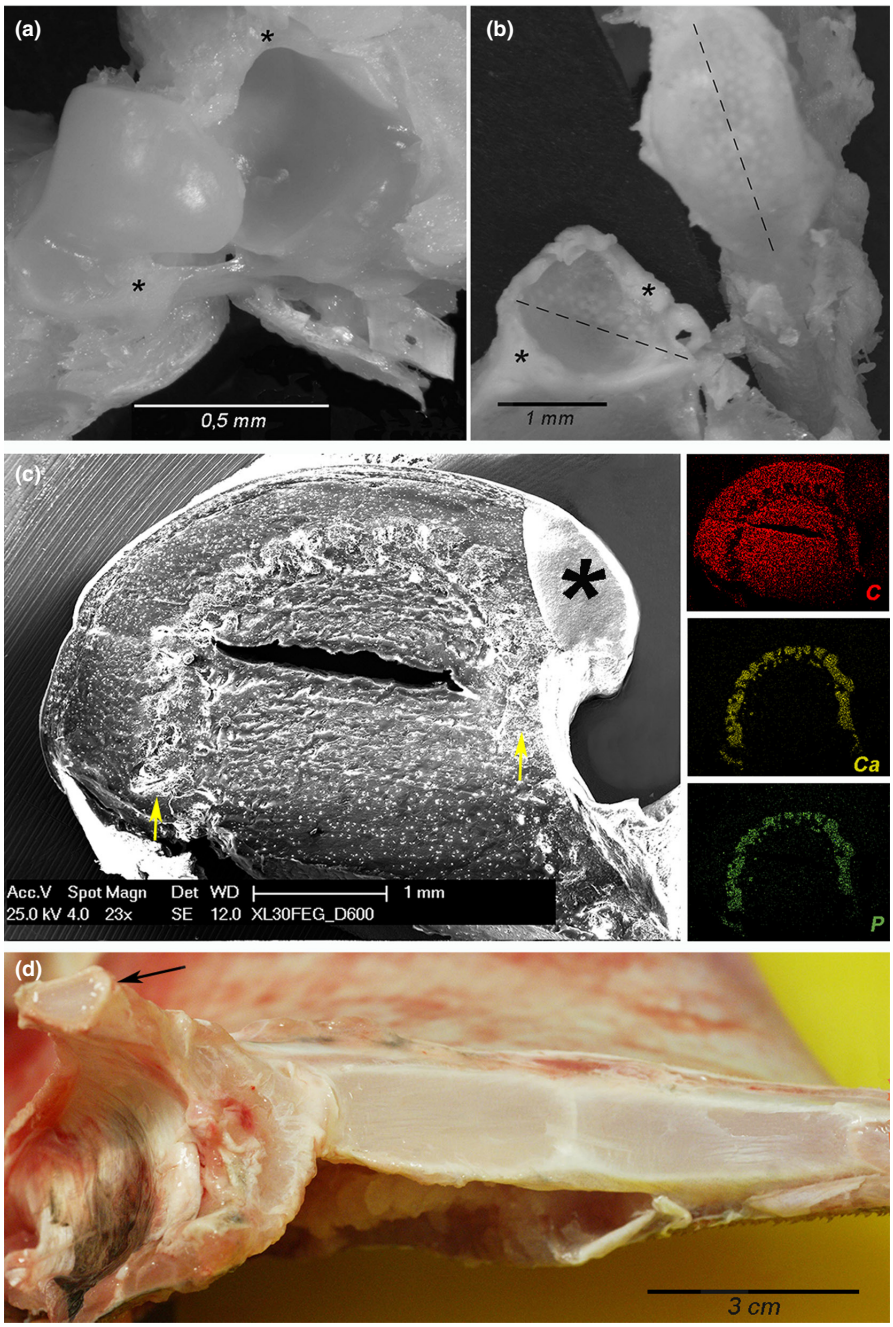

FIGURE 4 *Raya* cf. *polystigma*. (a, b) Macrodissection of the ball-socket (a) and condylar (b) joints showing the articular cavity, the capsule insertions (asterisks), and the mineralized tesserae which can be observed in transparency through the layer of hyaline cartilage. (c) SEM-BSA, magnification 23x and EDAX analysis. The transverse section of the pelvic girdle ball-socket joint shows a thin band of fibrous cartilage which leans on a thicker layer of uncalcified hyaline cartilage with globular chondrocyte lacunae; the below layer consists of calcified tesserae (arrows) as documented by EDAX analysis, while the central core is formed by uncalcified cartilage with globular chondrocyte lacunae. The fissure in the central core is an artifact of processing as well as conductive resin drop in the right corner (asterisk). (d) Macro dissection of the thoracic girdle and the right metapterygium medial surface showing the segmental pattern with interposed amphiarthroses. The left metapterygium has been removed evidencing the condylar joint surface (arrow)

2.3 | Scanning electron microscopy (SEM)

The SEM sections were cut perpendicularly and longitudinally to the endoskeleton segments using a scalpel. These were ultra-sonicated in a buffered pH 7.4 saline solution bath until clear of mechanical manipulation debris and kept in a 6% Na_3PO_4 solution (pH = 9.1) at 30°C for 1 min (Congiu & Pazzaglia, 2011). Specimens were dehydrated in increasingly concentrated ethanol solutions, critical point dried in a CO_2 environment, and coated with a thin layer of gold in a sputter coater (Emitech). Observations were conducted using a Philips XL30 scanning electron microscope (Philips) equipped with an EDAX analyzer.

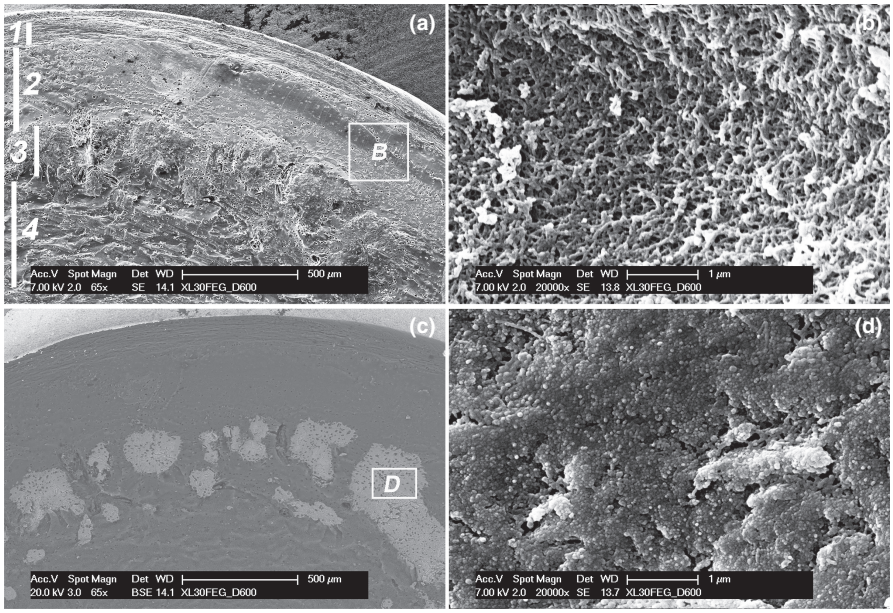

FIGURE 5 *Raja* cf. *polystigma*. (a) SEM, magnification 65x. Details of the joint cartilage structure: 1, layer of fibrous cartilage with flattened lacunae parallel to the joint surface; 2, layer of cartilage with globular lacunae; 3, layer of calcified tesserae; 4, central core uncalcified cartilage. (b) SEM, magnification 20,000x. The uncalcified matrix (corresponding to the square of b) forms a 3D network of collagen fibrils leaving interfibrils empty spaces. (c) SEM-BSA, magnification 65x. The same field of A in backscattered mode shows the calcified matrix of the tesserae with an irregular distribution of chondrocyte lacune and areas deprived of lacunae. (d) SEM, magnification 20,000x. In the calcified matrix (corresponding to the square of c), the fibrillar network is masked by densely packed globular material filling all the spaces between the fibrils

3 | RESULTS

3.1 | Diarthrodial and amphiarthrodial joints

The X-ray survey of the *Raja* cf. *polystigma* skeletons showed a large number of diarthroses and amphiarthroses which provided different degrees of movement between the neighboring calcified segments. The main diarthroses were observed between the upper and lower jaw, hyomandibula, dorsal girdle—propterygia and metapterygia; pelvic girdle—compound basals, pelvic girdle—basipterygia, and all basipterygia segments. Amphiarthroses joined segments of propterygia and metapterygia, the first row of radials with metapterygia and between the aligned radials in the fins (Figure 3a–c).

In this study, the diarthroses (dissected under the stereo microscope) show a single joint cavity surrounded by a fibrous capsule and the joint surface appears smooth and wet, revealing white spots of calcification below the surface (Figure 4a,b). The pelvic girdle-compound basal joint has a ball-socked shape resembling the inverted hip joint of a tetrapod and provides a 3D freedom of movement in the space (Figure 4c), while the pectora girdle—propterygia and metapterygia and pelvic girdle—basipterygia have a condylar shape with greater freedom of movement in the plane of the major diameter of the joint cavity (Figure 4b). The SEM sections were taken perpendicular to the ball or the condylar joint surfaces document a sequence of four layers: the outermost layer consists of a thin band of fibrous cartilage with flattened chondrocyte lacunae parallel to the joint surface, which leans on a thicker layer of the uncalcified matrix with globular chondrocyte lacunae (layers 1 and 2 of Figure 5a). The third layer is formed by calcified tesserae, as documented by SEM sections in BSA mode and the corresponding EDAX analysis (Figures 4c and 5c). The tesserae are also evident in transparency on the exposed joint surface of the fresh tissue specimens (Figure 4a,b). The inner core of the ball and condyles showed a texture of uncalcified cartilage with a regular distribution of globular chondrocytes. The macrodissection of tendons and muscles also exposed the line of insertion of the joint capsule (Figure 4a,b). Propterygia and metapterygia are formed by three to five elements joined by tight, fibrous amphiarthroses without any freedom of movement (Figure 4d). Amphiarthrodial joints between pterygia—radials first row and the lined-up radials of the wing fins are reported in the general context of the skeletal architecture of the wings.

3.2 | Wing-fin radials morphology

Radials are long and narrow cartilage elements aligned in straight lines in the wings of a flattened biconvex shape (perpendicular to the wing surface) and with pointed or rounded upper and lower borders (Figure 6a–c). One or more central columns of calcified cartilage run through the entire length of each radial, surrounded by an uninterrupted layer of uncalcified cartilage. The mineralized axis

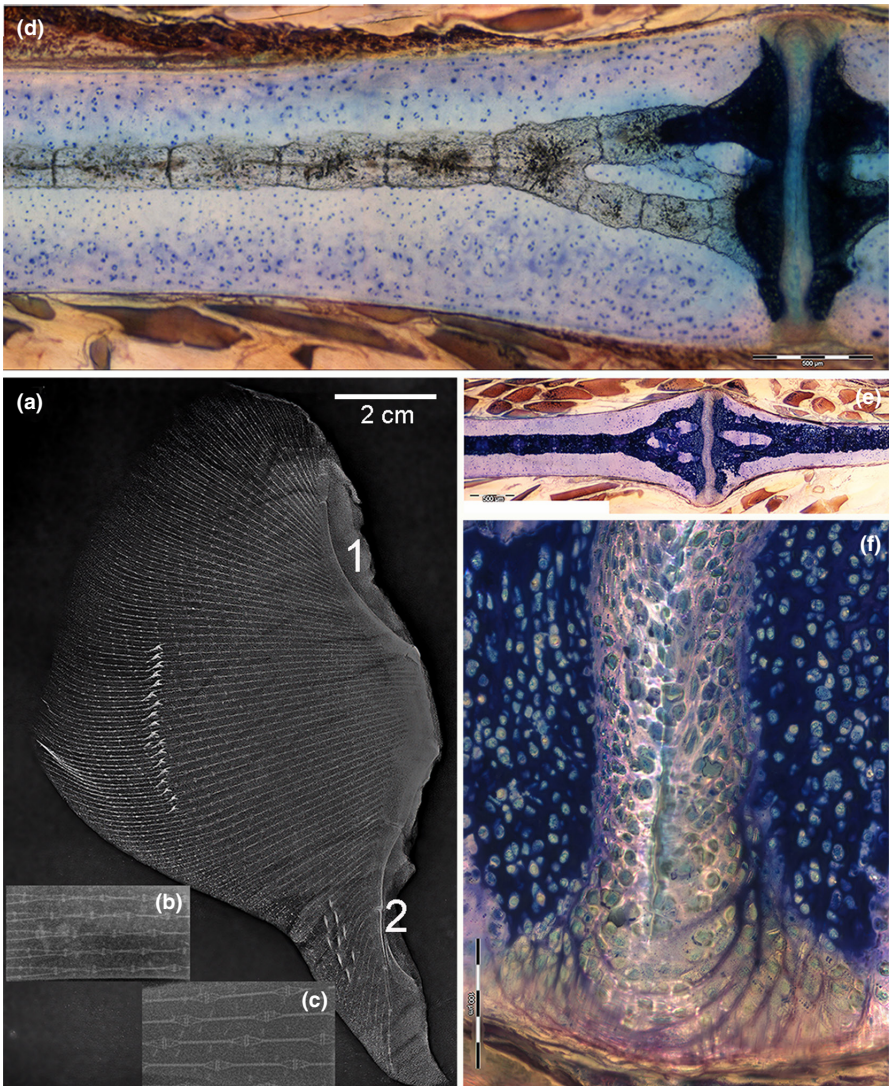

FIGURE 6 Radials structure of *Raja* cf. *polystigma*. (a) X-ray of the left wing showing calcified, parallel lines of thin segments perfectly aligned (radials). Bifurcations occur at about two-third of the line length. A stripe of calcified dermal denticles on the dorsal surface is superimposed in the image to the wing endoskeleton. The most medial band of radials forms joints with the propterygium (1) and metapterygium (2). (b, c) High-resolution X-rays of the radials central column (calcified) and interradial joints. (d, e) Resin-embedded, thick section, methylene blue-acid fuchsine, 10x. The calcified, central column of the radial is formed by a regular sequence of cylindrical sub-units which broach off at the extremity to support the flat disk of the inter-radial joint. The column is surrounded by a ring of uncalcified cartilage (difference of calcified cartilage staining discussed in the text). (f) Resin-embedded, thick section, toluidine blue-acid fuchsine, 200x. An uncalcified layer of densely packed chondroid-like cells (thickness about 100 μm) fills the joint space between the terminal disks supported by the column branches. The outer surface of these amphiarthroses is strengthened by arched collagen fibers

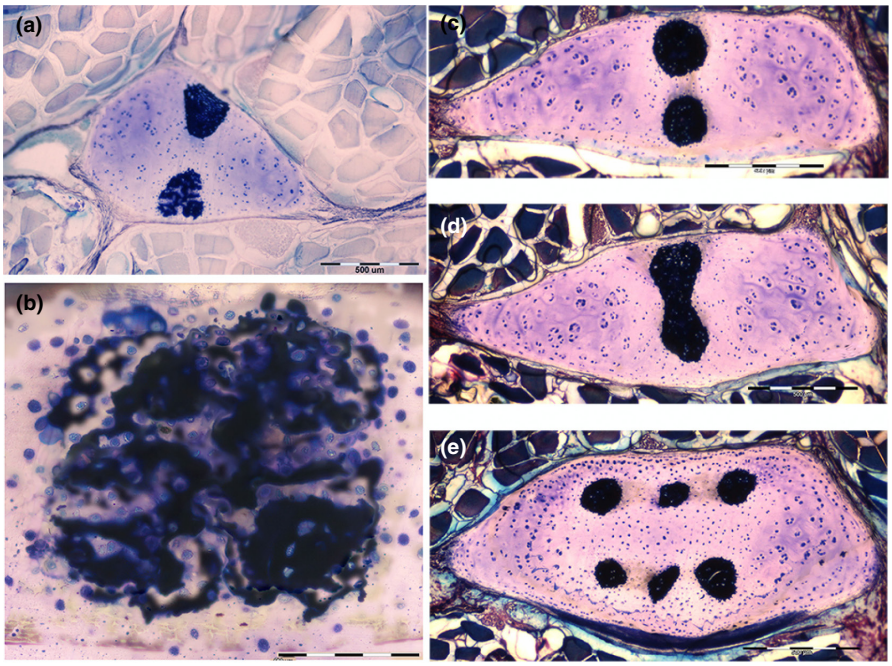

FIGURE 7 Radials structure of *Raja* cf. *polystigma* in transverse sections. (a) Resin-embedded, thick sections, toluidine blue-acid fuchsine, 10x. Radial with two calcified columns, one showing a less-advanced mineral deposition in the cartilage. (b) Detail at higher magnification of A, 400x. This column shows zones of higher mineral density (dark blue) mixed with zones of the uncalcified or partially calcified (faint blue) matrix. (c–e) Resin-embedded, thick sections, toluidine blue-acid fuchsine, 10x. Double, completely mineralized columns, a fusion of columns, and a radial with six columns

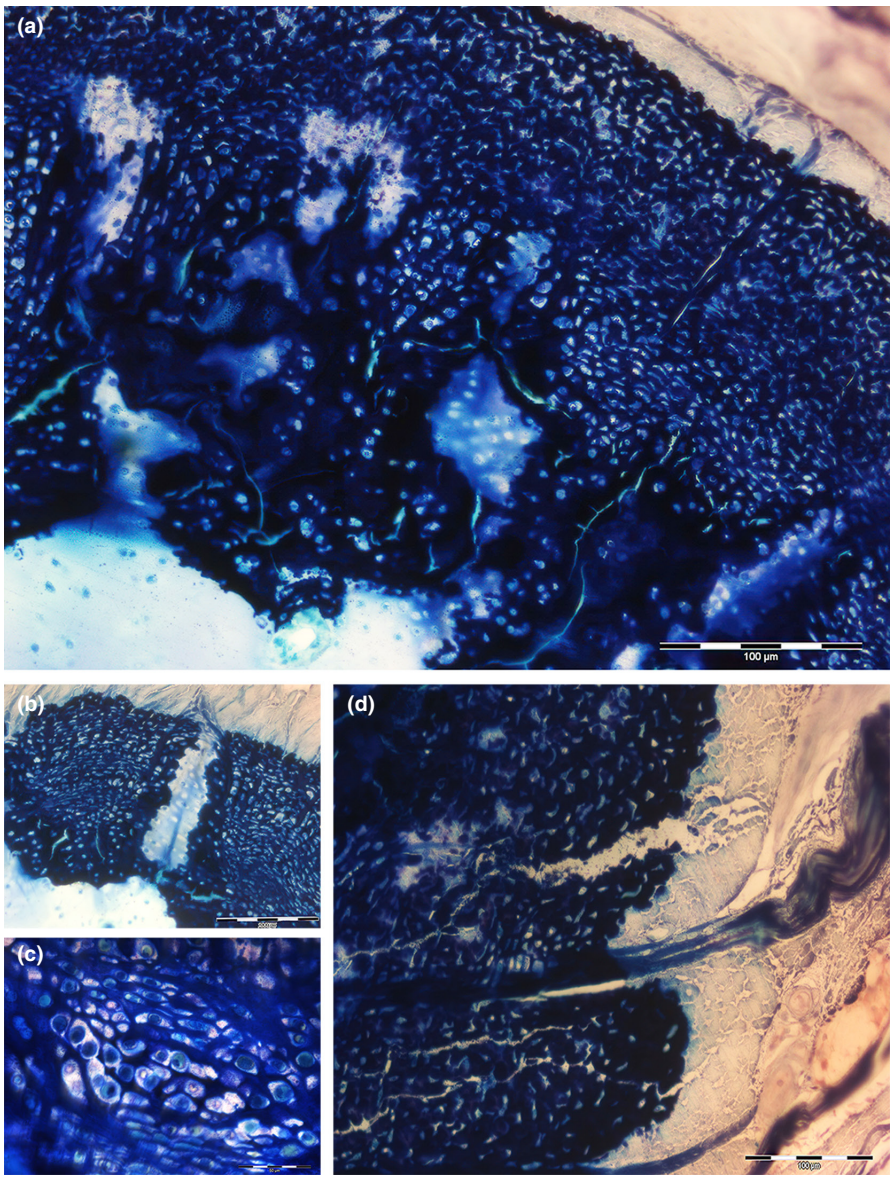

FIGURE 8 Tesseral histomorphology of the pelvic girdle and compound radial of *Raja* cf. *polystigma*. (a) Resin-embedded thick section, methylene blue-acid fuchsine, 200x. Scattered uncalcified zones and different mineralization densities in the tesseral layer of the pelvic girdle. (b) Resin embedded thick section, methylene blue-acid fuchsine, 40x. Intertesseral canal with uncalcified cartilage matrix of the tessellated layer of the compound radial. (c) Resin-embedded thick section, methylene blue-acid fuchsine, detail of A. Lacunae of the calcified matrix with duplicated chondrocytes. (d) Resin-embedded thick section, methylene blue-acid fuchsine, 200x. Sharpey fibers seep into the tessellated layer of the pelvic girdle

consists of a sequence of regular subunits that share the same basic morphology with the *tesserae* on the periphery of the endoskeleton segments (later reported). At the extremities of each radial, the central, mineralized column branches off in three or more diverging segments, which supports the flat calcified basis of the joint (Figure 6d,e), whose space is filled by an uncalcified layer of densely packed, chondroid cells with scanty intercellular matrix and occasionally showing a thin transverse cleft. Arched collagen fibers reinforce the external wall of the joint (Figure 6e,f). Up to 25 aligned radials spreading from the propterygia and metapterygia can be counted in the anterior wing fins. The thickness of the mineralized radial columns decreases from the medial to the outer band, while a bifurcation occurs at approximately two-thirds of the entire ray length, just medially to the line of dermal denticles in the middle part of the fin (Figure 6a). Radials spreading from the basipterygia segments 2 and 3 have a lower number of elements (≤10), the ray line is shorter than in the wings, and each radial can contain two or more mineralized columns (Figure 7c–e).

The longitudinal, resin-embedded radial thick sections (cut in a plane parallel to the long axis of the mineral columns) can be focused on a stained or deeper, the unstained plane of the mineralized column (an effect due to the limited infiltration depth of the staining solution in the resin). This histologic method provides clear evidence of the mineralized cartilage structural pattern,

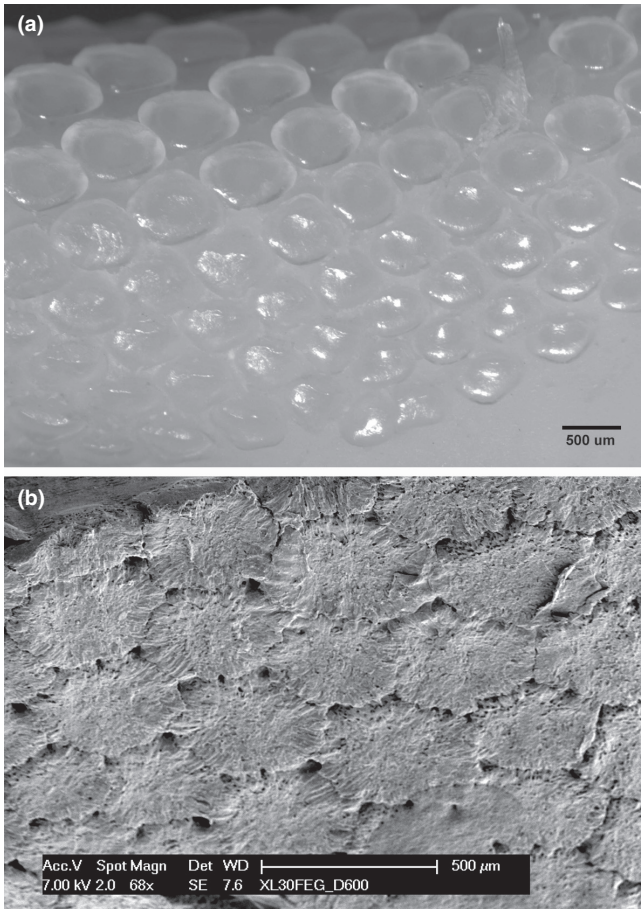

FIGURE 9 Compound radial, tessellated outer surface of the fresh tissue specimen and the corresponding area processed for SEM in *Raja* cf. *polystigma*. (a) The fresh specimen tesserae document an oval shape with rounded borders, separated by intertesseral transparent tissue. (b) Dehydrated and SEM processed tesserae appear densely packed and with polygonal shape, delimiting large pores in correspondence of the corners and smaller holes on the surface. Calcified crests can be observed to join neighboring tesserae

which shows a regular line of units with a repeated, inner organization (Figure 6d,e) that resembles the peripheral tesserae of the endoskeleton but aligned vertically rather than spread on the surface.

3.3 | Tessellated and uncalcified central cartilage of the endoskeleton

In the rostrum, skull, upper and lower jaws, dorsal and pelvic girdles, propterygia, metapterygia, and all basipterygia segments, mineral deposition occurs at the periphery of the cartilage central body and is therefore different from the catenated pattern of the radial-calcified columns. In undecalcified thick sections, different patterns can be observed among the endoskeleton elements, some of which show a peripheral, continuous, and smooth layer of calcified cartilage, while others show the tile pattern of tesserae (Figure 2a), which documents specific differences in morphology between the single endoskeleton segments or differences due to age and size in the studied group of *Raja* cf. *polystigma* specimens. The latter can be summarized in the following typologies: (a) flat tesserae with a thickness of about 50 µm, melting in the basal layer or separated by a zone of the uncalcified matrix in contact with the perichondrial layer (Figure 2b); (b) tesserae forming a denser, basal layer of calcified cartilage with small, flattened chondrocyte lacunae and an internal part bulging into the central cartilage mass with larger chondrocytes inside globular lacunae (Figure 2c); and (c) tesserae with a very high chondrocytes density with stratification of flattened and globular lacunae (Figure 2d). The latter type of tesserae has developed a height of approximately 500 µm (10 and 3 times higher than types a and b, respectively). The stratification shows bands of large chondrocytes with globular lacunae between layers of squashed cells inside flattened lacunae. The observation of a scanty intercellular matrix and lacunae containing two chondrocytes or paired lacunae suggests that in these tesserae the cell metabolic activity is turned toward duplication rather than matrix synthesis. Another aspect is the presence of irregularly scattered areas of cellular, uncalcified cartilage in the tesseral body (Figure 8a–c). Tendon fibers from the external muscles deepened in the tesseral calcified layer with the typical Sharpey fiber morphology of bones (Figure 8d). No mineral deposits were observed in the central cartilage of all endoskeleton segments, which, on the contrary, showed recently duplicated chondrocytes forming isogenic groups with a high number of paired lacunae or single lacunae with two cells inside. The tissue does not show a capillary network; however, canals of approximately 50 µm in diameter have occasionally been observed below the external tesseral layer in our specimens, similar to those recently reported by Marconi et al. (2020).

Fresh tissue dissection removing muscles and tendons enables exposure of the outer, calcified surface (not dehydrated and unstained), where the tesserae look like a regular sheet of oval-shaped units, well separated from each other by a transparent tissue (Figure 9a). Otherwise, the homologous surface processed and observed with SEM exhibits a sheet of densely packed, flat, polygonal units with cribriform surfaces, intertesseral fissures and larger holes corresponding to the polygon corners. A random distribution of strips of calcified material formed links between adjacent tesserae (Figures 9b and 10).

3.4 | SEM

The fractured cartilage surface of the endoskeleton segment's central core highlights the chondrocyte lacunae of globular shape, and some of them remain with the cell inside (Figure 11a). The chondrocytes showed a dense, superficial layout of fine processes pulled from the lacunar surface by processing manipulations; however, a few, thin filaments maintained contact with the underlying collagen network (Figure 11b). The bottom of the chondrocyte lacuna at

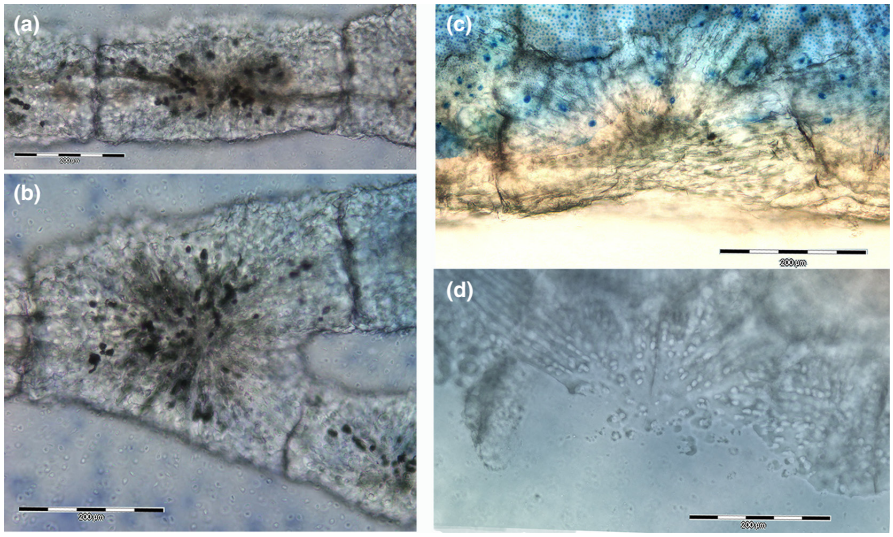

FIGURE 10 Mineralized scaffold comparison of radial columns and *tesserae* of *Raja* cf. *polystigma*. (a, b) Resin-embedded thick section, methylene blue-acid fuchsine, 100x. The column consists of aligned, cylinder-shaped segments (a) and branching units below the interradial joint (b). (c, d) Resin-embedded thick section, methylene blue-acid fuchsine and phase contrast, 100x. Tesserae show a polygonal shape with the same mineralization pattern of column subunits (c), while phase-contrast image (d) gives a higher definition of calcified cartilage canals formed by a pyle of aligned chondrocytes with an outer coating of mineral deposits

higher magnification highlights the 3D texture of the collagen fibril matrix (Figure 11c), in contrast to the corresponding calcified matrix of the tesserae (Figure 5d).

3.5 | Morphometry

The comparison of the basipterygium ventral marginal segment and the two symmetric dorsal marginal segments with nontesselated, peripheral layers (analyzed in the same histologic slides of Figure 2a) documents a significantly higher thickness ($p < 0.001$) of the tesselated calcified surface (Table 1). The recently duplicated chondrocytes formed isogenic groups in the central core (Graphical Abstract, A-B); however, the chondrocyte density of the uncalcified subtesseral layer in the same transverse sections of the endoskeleton segment was not significantly different (Table 2). In the pelvic girdle, the chondrocyte density of type c tesserae was significantly higher ($p < 0.0001$) than that in the corresponding central core transverse section (Table 2).

4 | DISCUSSION

The diarthroses of vertebrates link neighboring elements of the skeleton, providing different types and ranges of movement in relation to the shape of the opposing surfaces and the restraints of the external tissue (capsule and ligaments). The general structure of those in the batoid *Raja* cf. *polystigma* does not differ much from the corresponding joint types of terrestrial tetrapods. However, microdissection of the inner spaces of these joints allowed observation from within the capsule surface, which did not show a smooth and glossy tissue coating, suggesting the lack of a synovial membrane. The articular cartilage layer in the tetrapod joints is marked by a joint cavity and the epiphyseal ossification center, while in the two studied specimens of *Raja* cf. *polystigma*, the articular cartilage leans on a scaffold of mineralized cartilage tesserae that surround the core of uncalcified cartilage. Therefore, the tessellated layer below the diarthroses completes the external coat of the endoskeleton segment, which is documented in the ball-joint between the pelvic girdle and compound radial but which is shared by the other diarthroses of the examined specimens of *Raja* cf. *polystigma*. The morphologic and structural similarities with the bony skeleton of terrestrial tetrapods suggest the same biomechanics of these joints and the adaptation of the cartilage calcification pattern (peripheral tesserae model) leaving a layer of hyaline cartilage on the surface exposed to frictional stress due to the walking mode displayed by skates (Lucifera & Vassallo, 2002; Macesic & Summers, 2012). Regarding the swimming mode, the periarthroses between the neighboring radials allow a tight range of movement. However, considering the high number of stiff radials and interposed periarthroses, this structural layout can grant the single fin and the entire wing "in toto" graded flexibility that "the majority of batoid fishes use to swim and fall on a continuum from undulatory to oscillatory locomotion" (Schaefer & Summers, 2005).

The complex and phylogenetic variability of the batoid wing skeletal structure has been extensively studied with high-resolution radiography by Schaefer and Summers (2005), who reported extensive interspecies and intraindividual variations in the mineralization pattern and joint arrangement of the wing skeleton among 56 batoids species. These authors have correlated with the wing mechanics of the batoid swimming mode. The morphology of

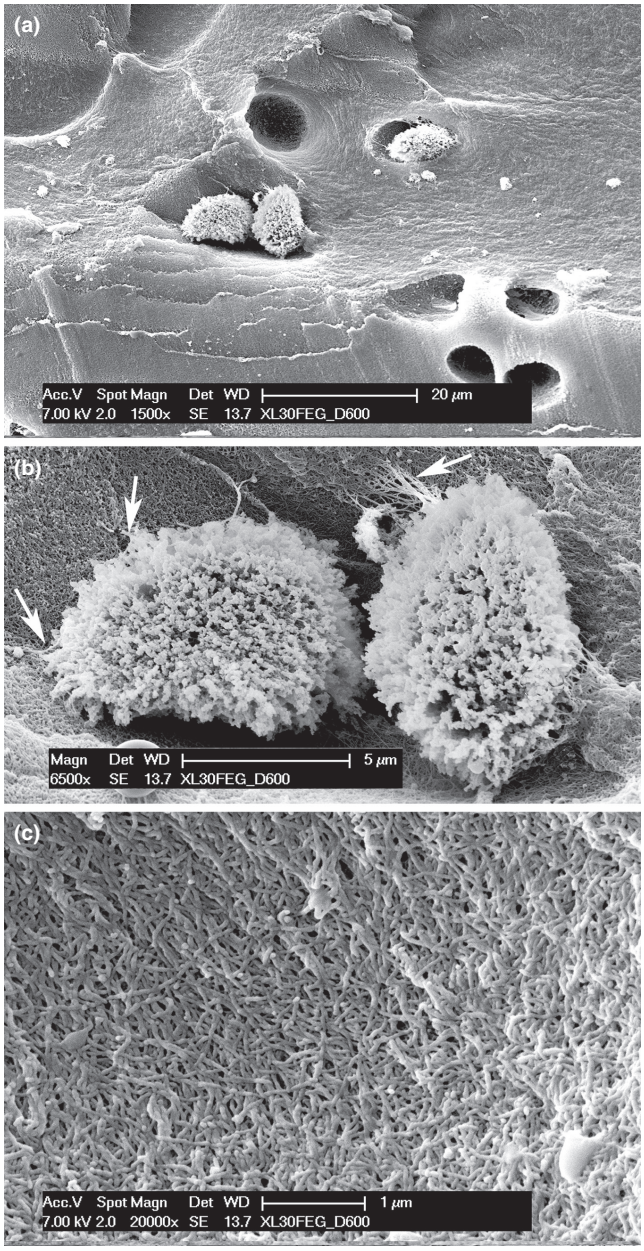

FIGURE 11 SEM fractured surface of metapterygium *tesserae* of *Raja* cf. *polystigma*. (a) Globular chondrocyte lacunae, in a few of them the chondrocyte has not been taken off by mechanical manipulation of processing. (b) Globular chondrocytes partially detached from their own lacuna. The cell surface presents a dense cover of the external membrane eversions, amputated in the specimen processing. However, a few of them have not been torn and maintain the connection with the spaces of the lacuna fibrils network (arrows). (c) Inner surface of a void chondrocyte lacuna showing the fibrils network of the uncalcified matrix

this study draws the attention to two, so far scarcely considered characters of the *Raja* cf. *polystigma* radials: (1) All of them (with the only exception of the compound radial) show one or more mineralized columns inside the cartilage body of the segment, in contrast with the other endoskeleton segments, where the calcified tesserae are placed as peripheral tiles. If it is single, the calcified column is positioned centrally in the cartilage body and, in this way, stiffens the long axis of the segment. Considering the wing X-rays and transverse sections, the calcified columns in the radials do not show appreciable differences in diameter, while the length is variable. Multiple columns can be observed in radials articulating with the metapterygia and basipterygia suggesting that the adopted morpho-functional strategy to increase the stiffness of the segment is to form more parallel columns rather than enlarging the size of the single center. (2) The thick, resin-embedded sections show the segmentation pattern of the mineralized columns with well-aligned units along the longitudinal axis of the radials. The microscopic structure of the calcified cartilage matrix is the same as that observed in the tesserae, but with a clear difference in shape and layout, the first being cylinder-like and regular with a constant circumference; the second because the units are tightly superimposed forming a column-like pyle.

The tesserae of elasmobranch fishes are defined as "abutting, mineralized, hexagonal blocks that overlay the central core of uncalcified cartilage," and Dean et al. (2009) extensively documented the ontogeny of the tessellated skeleton in the round stingray *Urobatis halleri* with cryo-SEM that correlates the growth of this species with the chondrocyte and tesserae morphometrics. A variety of morphological and imaging techniques have also been employed to overcome the difficulties linked to the analysis of these biological matrices, which mix soft and hard calcified tissues up to the ultrastructural level (Clement, 1992; Dean & Summers, 2006; Dean et al., 2005; Kemp & Westrin, 1979; Maisey et al., 2020; Seidel, Blumer, et al., 2020; Seidel, Jayasankar, et al., 2020) and to provide a solution to the conundrum of growth in an endoskeleton with external mineralization and no remodeling.

Regarding the basic question of chondrocyte proliferation and survival within a calcified matrix, the diffusion of fluids in the mineralized cartilage of the tessellated endoskeleton is still debated and is the key point for the explanation of the tessellated cartilage histomorphology. The structure of calcified tesserae in an adult stingray (*Urobatis halleri*) has been studied using synchrotron radiation microcomputed tomography (SR-μCT), which means the removal of most of the uncalcified cartilage in the specimen. This technique provided a 3D reconstruction with high resolution of the uncalcified spaces within the tesserae (Chaumel et al, 2020), allowing characterization of the variations of the tesseral shape and the arrangement of the lacunae which show a pronounced organization into parallel layers with a strong orientation of the neighboring tesserae toward the intertesseral pores. The proposed model is that of a network of lacunae linked by small passages (canaliculi) converging into the intertessera pores, where the latter represent the nutrient source for the chondrocytes embedded into the calcified matrix. The presence of canaliculi in the tessellated skeleton of *Chondrichthyes* has also been reported in an earlier study on the same stingray species using the cryo-SEM technique (Dean et al, 2010). Both studies suggest an extracellular fluid exchange that provides nutrient diffusion to chondrocytes with a similar lacuno-canalicular network and circulation of the cortical bone.

TABLE 1 Comparison of the mean height of the outer calcified cartilage layer between tessellated and not-tessellated elements of basipterygium segment 5 of *Raja* cf. *polystigma* (Figure 2a)

	Tesselated segment	Not-tesselated segment 1	Not-tesselated segment 2
n	50	64	58
mean height ± SD (μm)	91.28 ± 16.32	33 ± 10.90	29.70 ± 8.55
Tesselated segment	—	—	—
Not-tesselated segment 1	$p < 0.0001$	—	—
Not-tesselated segment 2	$p < 0.0001$	$p = 0.0642$	—

TABLE 2 Comparison in *Raja* cf. *polystigma* of chondrocyte lacunar density in the cartilage uncalcified core and subtesseral layer of metapterygium, in the uncalcified cartilage peripheral layer of radials and in the calcified type c tesserae of the pelvic girdle

	Uncalcified cart. central core (metapterygium)	Uncalcifield subtesseral layer (metapterygium)	Uncalcifield ext cartilage layer (radials)	Calfield cartilages (type c tesserae)
n	28	32	32	15
mean density ± SD (in fields 0,14 mm^2)	52 ± 7.07	55.31 ± 7.63	71.87 ± 10.95	274.8 ± 46.22
	Uncalcified cart. central core (metapterygium)	**Uncalcifield subtesseral layer (metapterygium)**	**Uncalcifield cartilage layer (radials)**	**Calfield cartilages (type c tesserae)**
Uncalcified cart. central core (metapterygium)	—	—	—	—
Uncalcifield subtesseral layer (metapterygium)	$p = 0.088$	—	—	—
Uncalcifield cartilage layer (radials)	$p < 0.0001$	$p < 0.0001$	—	—
Calfield cartilage (type c tesserae)	$p < 0.0001$	$p < 0.0001$	$p < 0.0001$	—

However, scant attention has been paid to the effects of dehydration and, in general, of processing electron microscopy imaging of the morphology of the specimens. In this study, an example is given by the dissected fresh tissue outer surface of the compound radial compared with the corresponding SEM image, where the tesserae show a regular oval shape with rounded borders rather than polygonal, densely packed, and sharp-edge units. The histology carried out on decalcified sections or resin-embedded, undecalcified sections confirmed the previously reported local variations in the size, form, and density/volume of chondrocytes, including zones of the acellular matrix (Seidel, Jayasankar, et al., 2020). These variations, when observed in single-species studies, can be related to specific characteristics of the endoskeleton segments and growth, while interspecies variations with typization of endoskeleton mineralization as reported by Seidel, Blumer, et al., (2020) can be used to distinguish the chondrichthyan phylogeny. In this study, particular attention has been paid to the density parameter of chondrocytes and associated mineral deposition processes. No significant differences in chondrocytes density have been observed between the central core, the subtesseral layer in the endoskeleton segments of *Raja* cf. *polystigma*, and in the outer uncalcified layer of radials, suggesting a regular interstitial growth pattern of the cartilage. By contrast, a highly significant difference in chondrocyte density has been documented in the large, mineralized type **c** tesserae of the pelvic girdle, suggesting a very high proliferation rate of these chondrocytes associated with a scarce or null synthesis of intercellular matrix. The alternate layers of globular and flattened chondrocyte of type c tesserae can be explained by recurrent phases of the fast duplication rate of chondrocytes (the large cells layer), while in the sectors where the replication process has stopped, the cells and the corresponding lacunae appear squashed and densely packed. In addition, the mineral deposition process also appears to be conditioned by the fast cell replication mode, because in these, zone matrix synthesis is slowed down and the basic fibril scaffold for crystal nucleation is reduced. This observation is also supported by the morphology of type b tesserae, the expression of a more mature growth phase with a basal, compact layer of mineralized cartilage with residual traces of flattened lacunae and an overlapping cup with globular chondrocytes and lacunae. This pattern can provide a satisfactory explanation of the morphology documented by light microscopy of resin-embedded, undecalcified sections showing a mix of the calcified and uncalcified matrix. However, the true question is how a quota of chondrocytes can survive in partially calcified tissue similar to tesserae.

There are little data on the postembryonic growth pattern of the tessellated endoskeleton segments of chondrichthyan, perhaps due to the general difficulties in locating and maintaining a suitable range of adult life stages, considering that these fish continue to grow throughout their lives. This paper documents the coexistence of two growth patterns in the adult *Raja* cf. *polystigma*: the first in the uncalcified hyaline cartilage core left out by the mineral deposition process and the second in the peripheral layer, where the tesserae increase the size and modulate the shape of the phasic chondrocyte proliferation associated with mineral deposition.

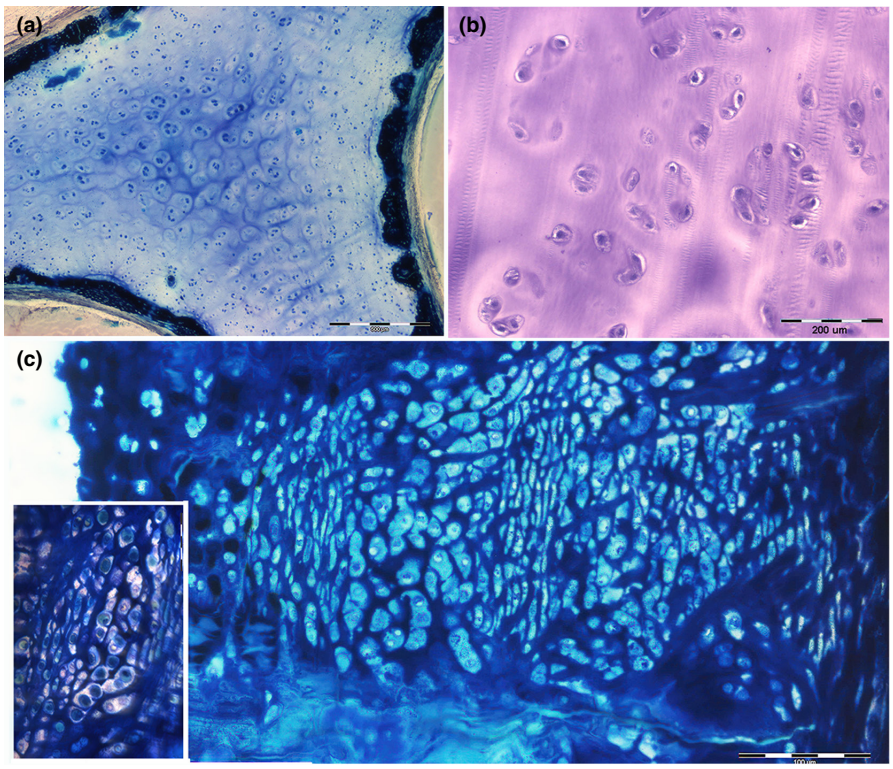

FIGURE 12 Summary of chondrocyte proliferation patterns and mineral deposition. (a) Resin-embedded, thick section, methylene blue, 40x. The transverse, undecalcified section of the metapterygium shows the chondrocytes proliferation forming isogenic groups in the central, unmineralized core. The outer calcified layer is formed not only by type a tesserae but also by segments of not-tessellated coating. (b) Paraffin-embedded, thin section, hematoxylin–eosin, 100x. Detail of chondrocytes isogenic groups in the central core. (c) Resin, thick section methylene blue, 200x Transverse section of the pelvic girdle showing a type c tessera abutting toward the central core. Stratification of flattened and globular lacunae. Most of the latter with a chondrocyte inside. The detail in the bottom-left corner shows the nonhomogeneous mineral density of the inter-lacunar matrix

The complex morphology of the tessellated layer, mixing zones of uncalcified cartilage, calcified cellular cartilage, and calcified matrix devoid of chondrocytes show the dynamics of a system that achieves a compromise of growing, living tissue with structural stiffening by the inorganic component as an alternative to bone remodeling developed in mammals. Therefore, a more complete understanding of this system dynamics is based on the key point of fluid diffusion in the endoskeleton segment. The observation of fissures or passages connecting the lacunar spaces within the tesserae, indicated with the term "intratesseral canaliculi" by Dean et al. (2009), has been hypothesized to be a way of extracellular fluid exchange and transmission of nutrients similar to the lacunocanalicular system of bone. However, to the best of our knowledge, to date, no evidence has been provided on chondrocyte processes, forming an intercellular network inside the mineralized tesserae, which would support a similarity to osteocytes. In a recent study, Marconi et al. (2020) documented in the skate *Leucoaja erinacea* cartilage canals (in the order size of 50 μm) passing through intertesseral joints and suggested that some chondrocyte progeny of the perichondrium are transported into the cartilage core along with this route to differentiate later into mature chondrocytes. In the present study, similar structures were occasionally observed in the subtesseral zone, but never reached the central cartilage core and did not seem compatible with the function of maintaining and nourishing the whole central core of the endoskeleton segments. The zonal, morphometric analysis carried out in this study showed a regular distribution of already differentiated chondrocyte duplications (isogenic groups and density of recently duplicated cells) in the whole area of the central cartilage, while fluid diffusion occurs through the fibrillar network of the uncalcified matrix but not through the calcified matrix of the tesserae. The diffuse chondrocyte proliferation and the ensuing increase in the volume of the central cartilage develop an eccentric force on the stiff and calcified border, explaining the diversified morphology of the tesseral layer, that mixes cartilage zones from uncalcified and mineralized matrix (cellular or acellular). In this model (Figure 12), the intertesseral joints can play a dual function: (a) mechanical, because they give a certain degree of resilience to the calcified, external border capable of balancing the growth of the central cartilage core and (b) biologic, because the scattered, uncalcified zones may allow fluid diffusion from the perichondrium and the general vascular circulation through the fibrils network of the matrix.

Further research is needed to address the questions posed not only by the differences in mineral deposition in the radial and endoskeleton segments of batoids but also by the peculiar relationship in type c tesseral growth between chondrocyte proliferation and

mineral deposition. A comparative analysis of the cartilage calcification pattern of mammals would help to improve the knowledge of both these models.

ACKNOWLEDGMENTS

The study was carried out using the SEM microscope of the University of Insubria and the light microscopy facilities of the University of Brescia, thanks to a research agreement between the two universities. This study was supported by current research funds from DMC at the University of Insubria. The senior author is a retired professor of Orthopedic Surgery from the University of Brescia. The authors acknowledge the contribution of the Committee of the Mario Boni Foundation of Pavia and the valuable support of Dr. Battista Galli, Clinica Veterinaria CMV of Varese for the X-rays documentation.

ORCID

Ugo E. Pazzaglia https://orcid.org/0000-0002-3344-2388
Mario Raspanti https://orcid.org/0000-0001-6322-1845

REFERENCES

Bland, J.M. & Altman, D.G. (2010) Statistical methods for assessing agreement between two methods of clinical measurement. *International Journal of Nursing Studies*, 47, 931–936.

Clement, J.G. (1992) Re-examination of the fine structure of endoskeletal mineralization in Chondrichthyes: implications for growth, ageing and calcium homeostasis. *Australian Journal of Marine and Freshwater Research*, 43, 157–181.

Compagno, L.J.V. (1999) Endoskeleton. In: Hamlett, W.C. (Eds). *Shark, skates and rays. The biology of elasmobranch fishes*. Baltimore: John Hopkins University Press, pp. 217–248.

Congiu, T. & Pazzaglia, U.E. (2011) The sealed osteons of cortical diaphyseal bone. Early observations revisited with scanning electron microscopy. *The Anatomical Record: Advances in Integrative Anatomy and Evolutionary Biology*, 294, 193–198.

Dean, M.S., Chiou, W.-A. & Summers, A.P. (2005) Morphology and ultrastructure pf prismatic calcified cartilage. *Microscopy and Microanalysis*, 11(suppl 2), 1196–1197.

Dean, M.N., Mull, C.G., Gorb, S.N. & Summers, A.P. (2009) Ontogeny of the tessellated skeleton: insight from the skeletal growth of the round stingray *Urobatis halleri*. *Journal of Anatomy*, 215, 227–239.

Dean, M.S. & Summers, A.P. (2006) Cartilage in the skeleton of cartilaginous fishes. *Zoology*, 109, 164–169.

Decker, R.S. (2017) Articular cartilage and joint development from embryogenesis to adulthood. *Seminars in Cell & Developmental Biology*, 62, 50–56.

Dooley, W.C., Roberts, J. & Allison, C. (1989) Acid Giemsa technique for rapid identification of mitotic cells. *Journal of Histochemistry and Cytochemistry*, 37, 1553–1556.

Hall, B.K. (2005) *Bones and cartilage: developmental skeletal biology*. London: Elsevier/Academic Press.

Kemp, N.E. & Westrin, S.K. (1979) Ultrastructure of calcified cartilage in the endoskeletal tesserae of sharks. *Journal of Morphology*, 160, 75–102.

Lucifora, L.O. & Vassallo, A.I. (2002) Walking in skates (Chondrichthyes, Rajidae): anatomy, behaviour and analogies to teorapod locomotion. *Biological Journal of the Linnean Society*, 77, 35–41.

Macesic, L.J. & Summers, A.P. (2012) Flexural stiffness and composition of the batoid propterygium as predictors of punting ability. *Journal of Experimental Biology*, 215, 2003–2012.

Maisey, J.G., Denton, J.S., Burrow, C. & Pradel, A. (2020) Architectural and ultrastructural features of tessellated calcified cartilage in modern and extinct chondrichthyan fished. *Journal of Fish Biology*, 2020, 1–23. Available from: https://doi.org/10.1111/jfb.14376

Marconi, A., Hancock-Ronemus, A. & Gillis, J.A. (2020) Adult chondrogenesis and spontaneous cartilage repair in the skate, *Leucoraja erinacea*. *Elife*, 9, e53414.

Pazzaglia, U.E., Congiu, T., Sibilia, V., Casati, L., Minini, A. & Benetti, A. (2017) Growth and shaping of metacarpal and carpal cartilage anlagen: application of morphometry to the development of short and long bones. A study of human hand anlagen in the fetal period. *Journal of Morphology*, 278, 884–895.

Pazzaglia, U.E., Reguzzoni, M., Casati, L., Sibilia, V., Zarattini, G. & Raspanti, M. (2020) New morphological evidence of the 'fate' of growth plate hypertrophic chondrocytes in the general context of endochondral ossification. *Journal of Anatomy*, 236, 305–316.

Pazzaglia, U.E., Reguzzoni, M., Pagani, F., Sibilia, V., Congiu, T., Salvi, A.G. et al. (2018) Study of endochondral ossification in human fetal cartilage anlagen of metacarpals: comparative morphology of mineral deposition in cartilage and in the periosteal bone matrix. *Anatomical Record*, 301, 571–580.

Schaefer, J.T. & Summers, A.P. (2005) Batoid wing skeletal structure: novel morphologies, mechanical implications and phylogenetic patterns. *Journal of Morphology*, 264, 298–310.

Seidel, R., Blumer, M., Chaumel, J., Amini, S. & Dean, M.N. (2020) Endoskeletal mineralization in chimaera and comparative guide to tessellated cartilage in chondrichthyan fishes (sharks, rays and chimaera). *Journal of the Royal Society, Interface*, 17, 20200474.

Seidel, R., Blumer, M., Pechriggi, E.-J., Lyons, K., Hall, B. K. & Fratzl, P. et al. (2017) Calcified cartilage or bone? Collagens in the tessellated endoskeletons of cartilaginous fich (sharks and rays). *Journal of Structural Biology*, 200, 54–71.

Seidel, R., Blumer, M., Zaslansky, P., Knotel, D., Huber, D.R. & Weaver, J.C. et al. (2017) Ultrastructural, material and crystallographic description of endophphytic masses – a possible damage response in shark and ray tessellated cartilage. *Journal of Structural Biology*, 198, 5–18.

Seidel, R., Jayasankar, A.K. & Dean, M.N. (2020) The multiscale architecture of tessellated cartilage and its reation to function. *Journal of Fish Biology*, 2020, 1–14. Available from: https://doi.org/10.1111/jfb.14444

Seidel, R., Lyons, K., Blumer, M., Zaslansky, P., Fratzl, P., Weaver, C. et al. (2016) Ultrastructural and developmental features of the tessellated endoskeleton of elasmobranchs (sharks and rays). *Journal of Anatomy*, 229, 681–702.

Serena, F., Mancusi, C. & Barone, M. (2010) Field identification guide to the skates (Rajidae) of the Mediterranean sea. Guidelines for data collection and analysis. *Biologia Marina Mediterranea*, 17 (suppl 2), 1–204.

How to cite this article: Pazzaglia, U.E., Reguzzoni, M., Manconi, R., Zecca, P.A., Zarattini, G., Campagnolo, M. & et al (2022) Morphology of joints and patterns of cartilage calcification in the endoskeleton of the batoid *Raja* cf. *polystigma*. *Journal of Anatomy*, 240, 1127–1140. Available from: https://doi.org/10.1111/joa.13623